Electronic Supplementary Material (ESI) for Journal of Materials Chemistry C.

Theoretical Discovery of half-metallic Dirac dispersion in experimentally synthesized two dimensional metal semiquinoid frameworks

Table S1. Energies for M-SF under different magnetic states (ferromagnetic (FM), antiferromagnetic (AFM), and nonferromagnetic (NM)). The bold energies are relatively lower in each configurations.

Energy (eV)	FM	AFM	NM
Ti-SF	**-281.027**	-280.944	-280.024
V-SF	-280.038	-280.230	**-280.329**
Cr-SF	-278.894	**-279.144**	-277.726
Fe-SF	**-273.192**	-272.759	-272.203

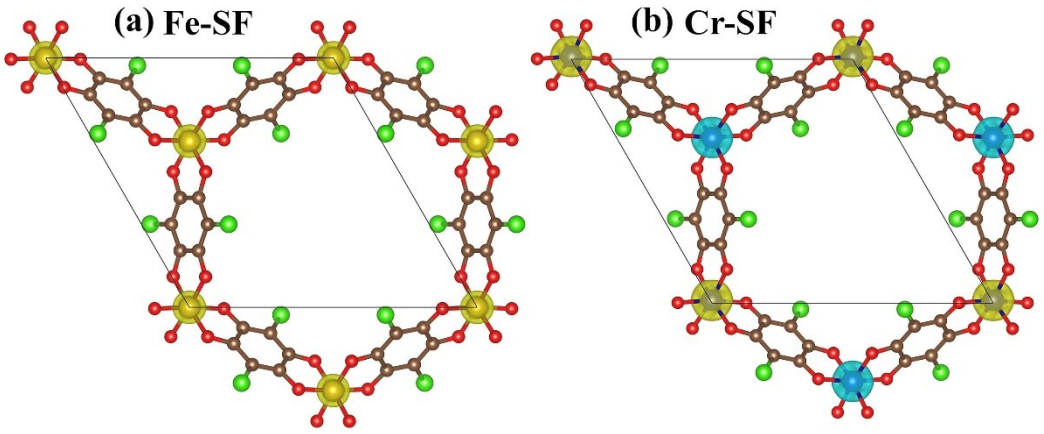

FIG. S1. The spin density of (a) Fe-SF (ferromagnetic) and (d) Cr-SF (antiferromagnetic) with isovalue of 0.02 e/ Å^3.

Thermodynamic stability

The thermodynamic stability was evaluated through Ab initio molecular dynamics (AIMD) simulations in a 2×2×1 supercell at room temperature (300K), based on the Nosé-Hoover method. The whole simulations last 10 picoseconds (ps) with a time step of 1 femtosecond (fs).

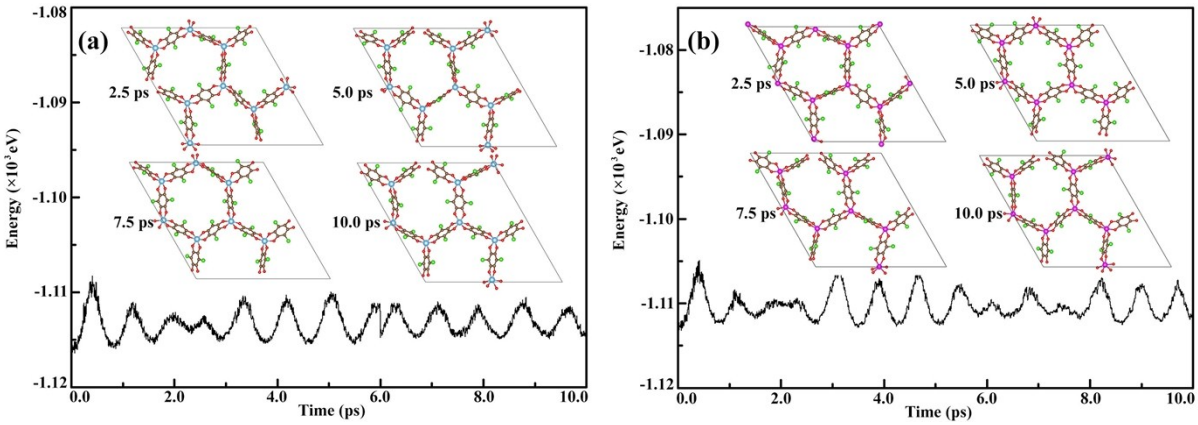

FIG. S2. Total potential energies of (a) Ti-SF, and (b) V-SF fluctuate during the AIMD simulation at 300K. The top view of Ti- and V-SF during the whole simulation are inserted in the pictures.

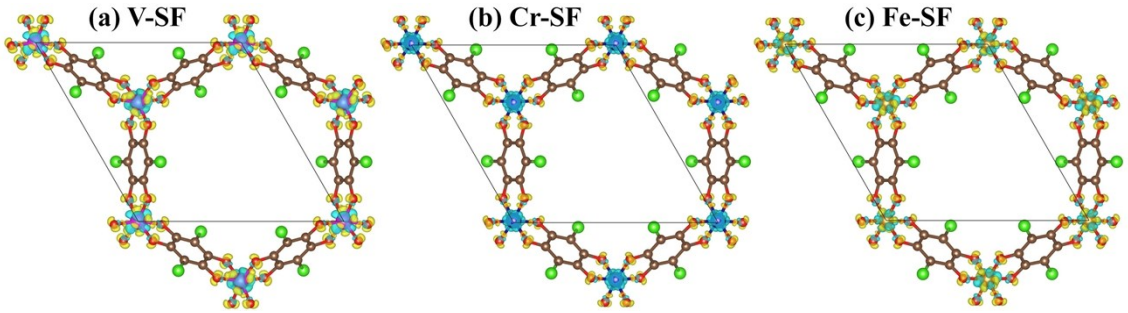

FIG. S3. Charge density difference for (a) V, (b) Cr, and (c) Fe-SF with respect to the metal atoms and ligands. The yellow and cyan region represent the electron accumulation and depletion area with an isovalue of 0.02 e/ $Å^3$.

Table S2. Bader charge analysis of M-SF.

	Average atomic charge (a.u.)		
	metal atom	O atom	C atom
Ti-SF	+1.90	-0.91	+0.05
V-SF	+2.14	-0.95	+0.44
Cr-SF	+1.81	-0.92	+0.42
Fe-SF	+1.55	-0.89	+0.39

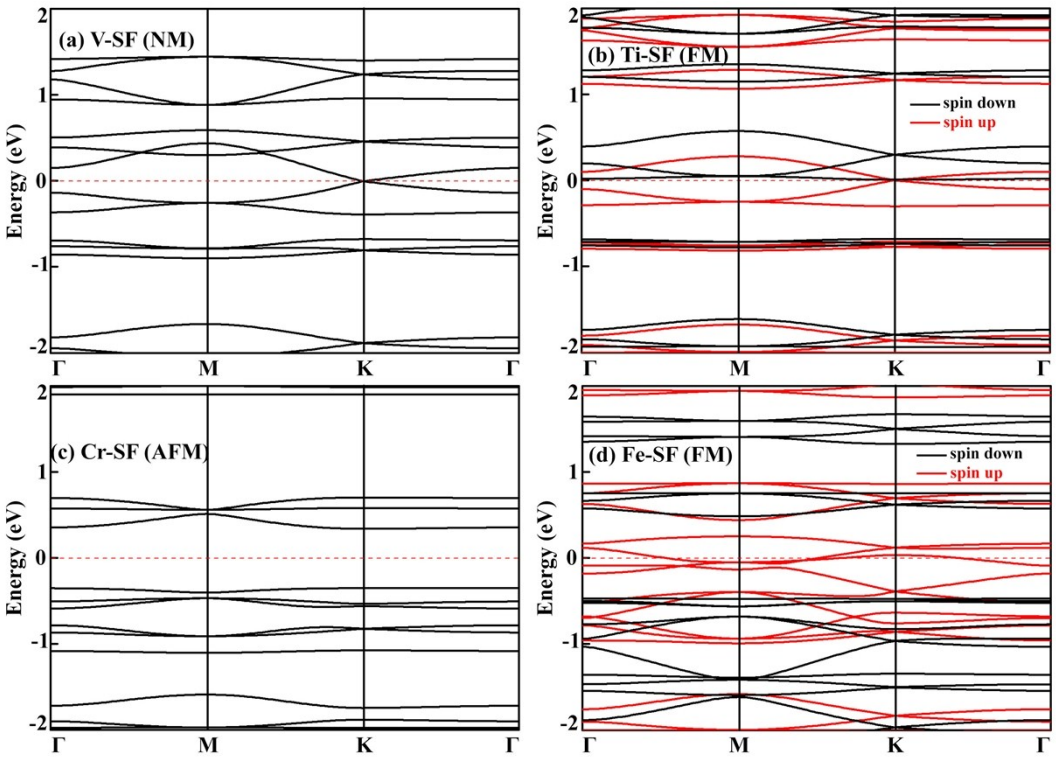

FIG. S4. Band structures of M-SF at magnetic ground states calculated by GGA_PBE functional.

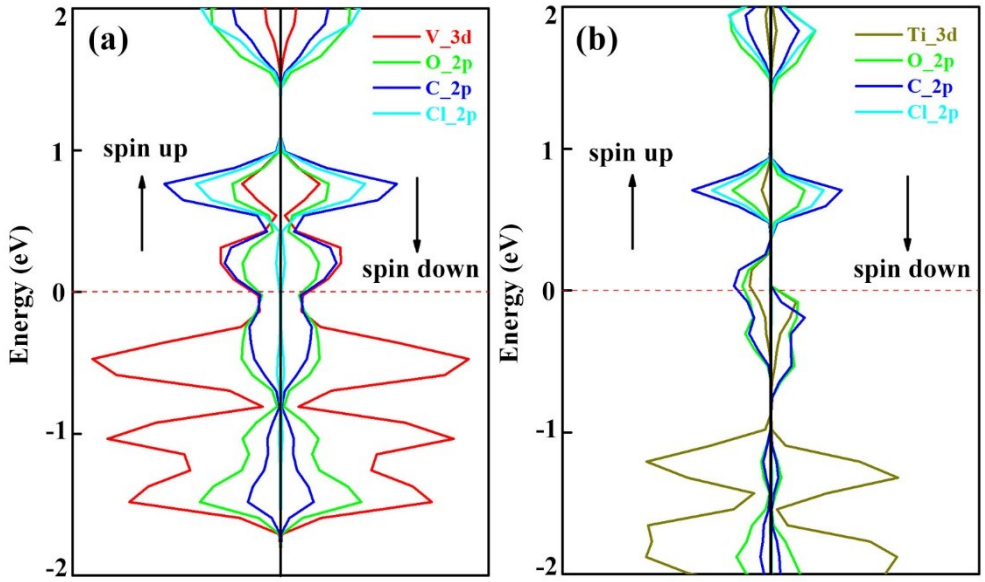

FIG. S5. Density of states of (a) V-SF and (b) Ti-SF. Fermi level (red dashed line) has been set to zero.

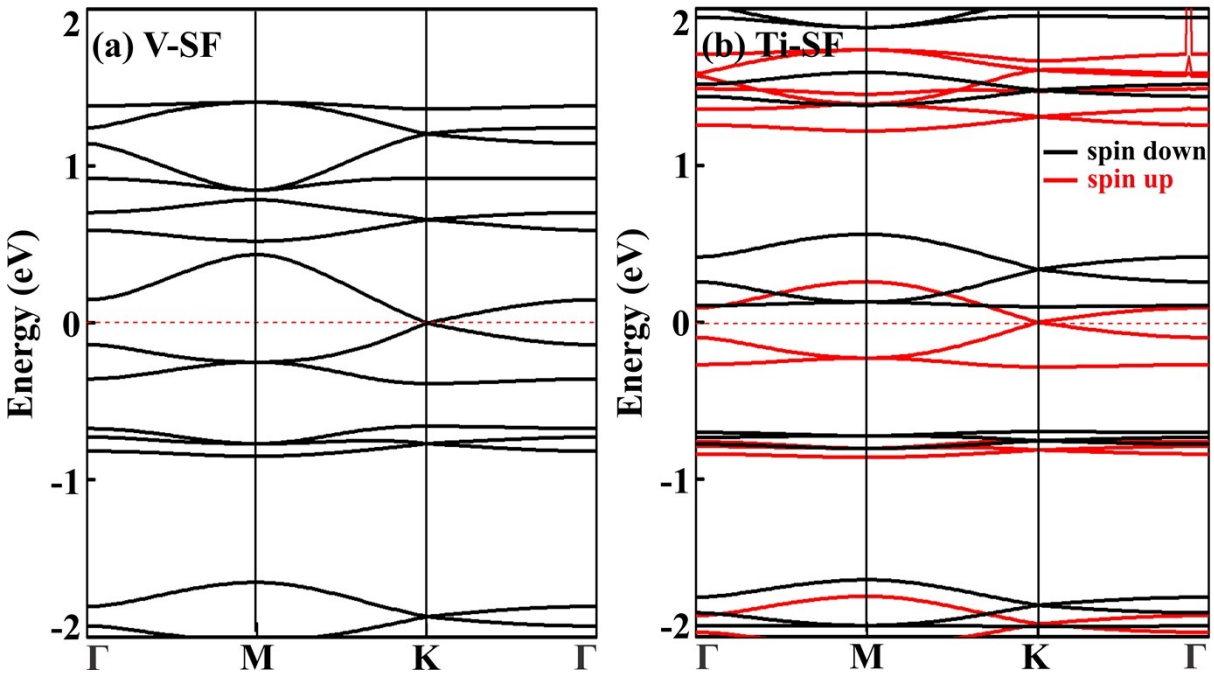

FIG. S6. Band structures of V-SF and Ti-SF at magnetic ground states calculated by GGA+U method, the U values are set to 2.0 eV for V, and 2.3 eV for Ti 3d orbitals[1].

Strain effect.

Generally speaking, the mechanical strength of M-SF is not very well, the critical breaking strain of V-SF and Ti-SF are 10% and 8%, respectively (Fig. S7). Therefore, we only employed a small biaxial strain (from -5% to 5%) in our band calculations. For V-SF, strains show little impact on Dirac points, only a bandgap of 5.0 meV opens under -5% compression. Whereas, for Ti-SF, small bandgaps appear under tension and -1% compression. It is noteworthy that the Dirac cones will be broken when the compression reaching -3% in Ti-SF, due to the rotation of organic ligands (Fig. S8). The fermi velocity of the conical bands under strains show on significant change in comparison with the full relaxed structures.

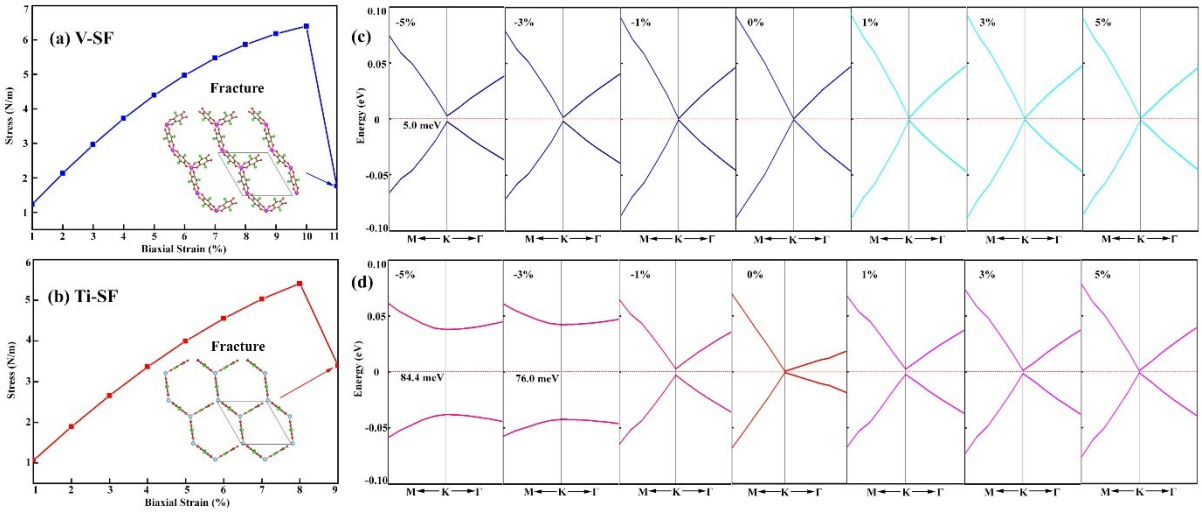

FIG. S7. Strains in the (a) V-SF and (b) Ti-SF subjected to biaxial strain. Band structures of (c) V-SF and (d) Ti-SF near K point under finite equal-biaxial strain. HSE functional is employed in band calculations. The fermi level (red dashed line) has been set to zero.

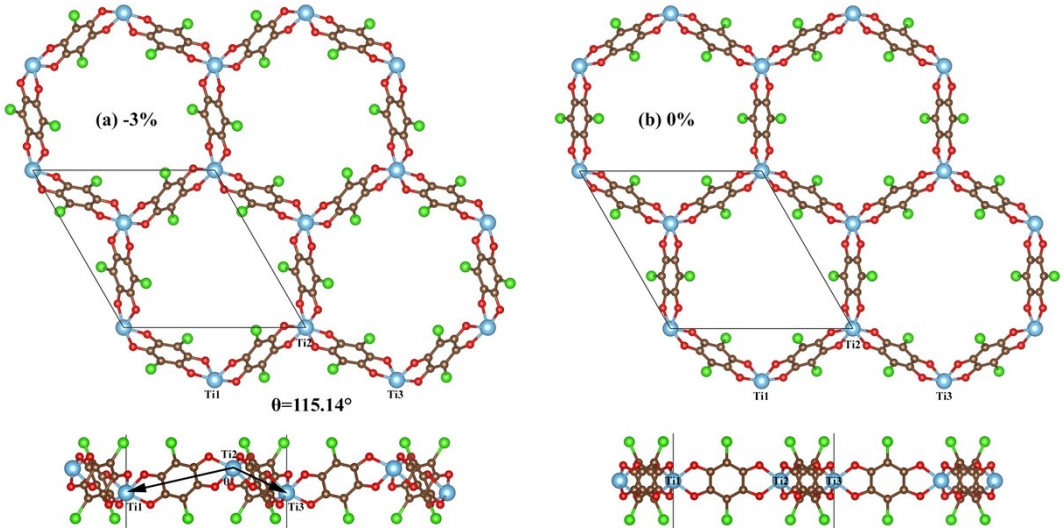

FIG. S8. The optimized structures of Ti-SF under the strain of (a) -3% and (b) 0%.

The calculation of exchange interaction (*J*)

For Ti-SF, the centre metal atoms (Ti) show ferromagnetic coupling with its neighbouring atoms. Here, to be simple, we regard the Ti atoms as the magnetic centre (Fig. S9), so that, Ti-SF will show similar magnetic structure with CrI_3.[2] According to Heisenberg model, the spin Hamiltonian can be written as:

$$H = -J \sum_{<i,j>} \sigma_i \sigma_j$$

where σ is +1 or -1 at each magnetic site. Thus, the energies for the magnetic configuration FM and AFM are derived as following equations:

$$E_{FM} = E_0 - \frac{3}{2} NJ|\sigma|^2$$

$$E_{AFM} = E_0 + \frac{3}{2} NJ|\sigma|^2$$

therefore,

$$J = \frac{E_{AFM} - E_{FM}}{3N|\sigma|^2}$$

where N is the number of the magnetic atom in the unit cell. E_{AFM} and E_{FM} represent the energies under AFM and FM magnetic order, respectively. Besides, on the basis of our DFT calculation, T_c for CrI_3 is 46 K, which is very close to the experimental value[3].

Tight binding model.

Due to the strong π-d conjugation and local charge density near fermi level, here we treated the central metals as the vertexes of a honeycomb sublattice, like the Carbon atoms of Graphene. Considering the hopping between nearest neighbors (site A and B), the TB Hamiltonian $H(\vec{k}) = \begin{pmatrix} \varepsilon & tf^* \\ tf & \varepsilon \end{pmatrix}$ leads to two energy eigenvalues

$$E_{1,2} = \varepsilon \pm t\sqrt{f(\vec{k}) \times f^*(\vec{k})}$$

with

$$f(\vec{k}) \times f^*(\vec{k}) = 3 + 4\cos\left(\frac{\sqrt{3}}{2}ak_y\right)\cos\left(\frac{3}{2}ak_x\right) + 2cos(\sqrt{3}ak_y)$$

and

$$t = \langle \varphi_A \left| H \right| \varphi_B \rangle$$

Then we fit our HSE band structures of V-SF and Ti-SF in the first BZ with our TB model.

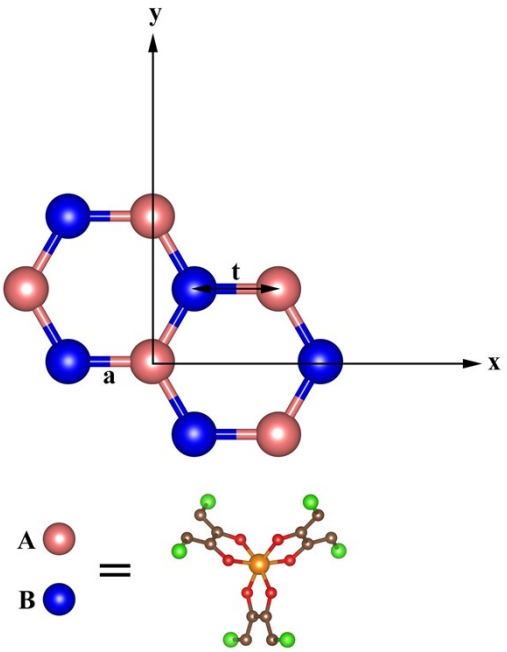

FIG. S9. Tight binding model for M-SF. Pink and blue balls represent different sites in the unit cell.

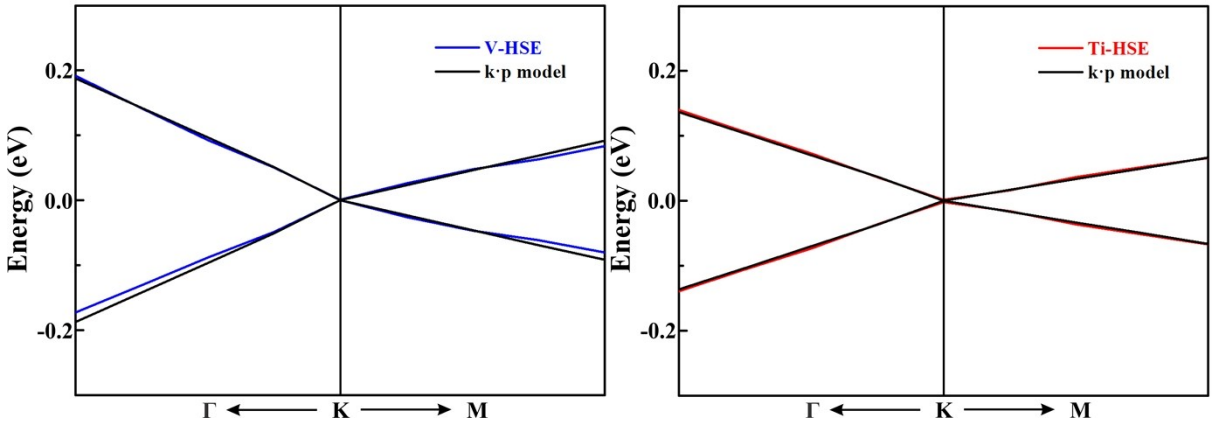

FIG. S10. Band structures of (a) V-SF and (b) Ti-SF calculated by HSE and *k·p* methods.

Molecular orbital model.

Inspired by the previous works[4-6], herein, we perfectly explained the magnetism of M-SF with a local D_3 symmetry at the metal-center, and successfully predicted the magnetism of unsynthesized metal-semiquinoid frameworks. First, we considered that the bonding π orbitals of organic ligands are full-filled, because the outmost orbitals of the ligand atoms are all over half occupied (non-metal atoms). Therefore, the orbitals with π features ought to be π^* orbitals of ligands[4]. Besides, as mentioned above, the highest valence band and lowest conduction band of M-SF ligands both show π* orbital feature, so that, we considered that these orbitals are half occupied. Previous works gave a simple combination of π^* and t_{2g} orbitals[5] (Fig. S11(a)). This molecular orbital model only can be used when the metal atoms have no more than 6 3d electrons. In order to predict the magnetism of all 3d transition metals, the combination of ligand σ and metal 4s and e_g orbitals should be involved. As an example, we exhibited molecular orbital model of V-SF and Co-SF. The previous model shows no single electrons in V-SF molecular orbitals, indicating its nonmagnetic properties, which also can be illustrated by our molecular model (Fig. S11(b)). However, through considering the interaction between ligand σ and metal 4s and e_g orbitals, our molecular orbital model can predict the magnetic state of metal-semiquinoid frameworks with all 3d transition metal center. Here we predicted that M-SF (M=Sc, V, Co, Cu) are all nonmagnetic, which can be confirmed by our DFT calculations (Table S3).

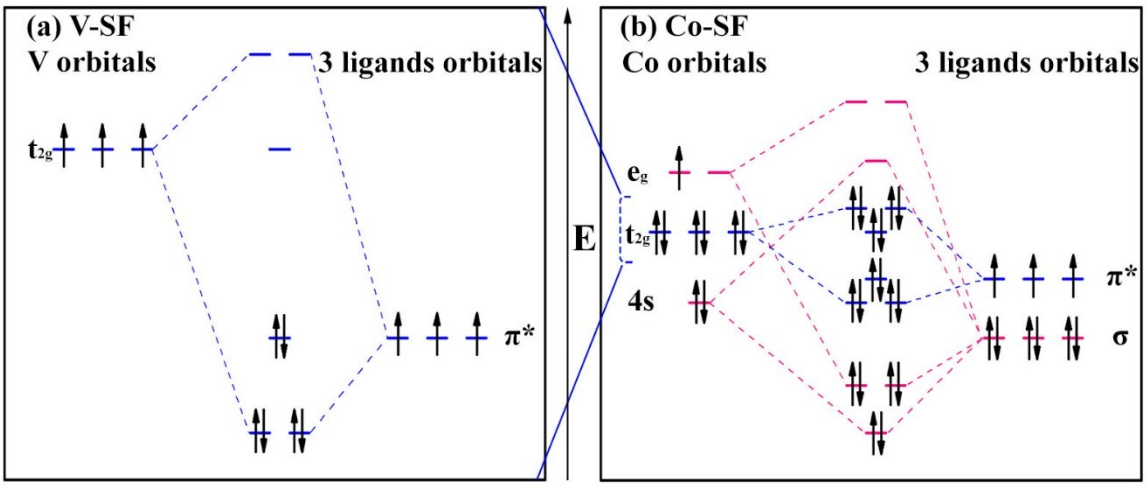

FIG. S11. Proposed molecular orbital model of (a) V-SF and (b) Co-SF with local D_3 symmetry at the metal center.

Table S3. Energies of M-SF (here, M represents all 3d transition metals) under different magnetic states (ferromagnetic (FM), antiferromagnetic (AFM), and nonferromagnetic (NM)). The magnetic moments ($M_{M\text{-}SF}$) under ferromagnetic state of them are shown in the table. The bold energies are relatively lower in each configurations.

	Energy (eV)			$\lvert M_{M\text{-}SF}\rvert$ (μ_B)
	FM	AFM	NM	
Sc-SF	-279.206	-279.729	**-279.731**	**0.0**
Ti-SF	**-281.027**	-280.944	-280.024	2.0
V-SF	-280.038	-280.230	**-280.329**	**0.0**
Cr-SF	-278.894	**-279.144**	-277.726	6.0
Mn-SF	-275.997	**-276.245**	-275.625	4.0
Fe-SF	**-273.192**	-272.759	-272.203	2.0
Co-SF	-269.509	-270.134	**-270.135**	**0.0**
Ni-SF	**-264.306**	-264.211	-264.304	2.0
Cu-SF	-259.241	-259.240	**-259.454**	**0.0**
Zn-SF	**-257.814**	-257.720	-256.484	2.0

Reference

1. S. Lutfalla, V. Shapovalov and A. T. Bell, *Journal of chemical theory and computation*, 2011, **7**, 2218-2223.
2. Y. Zhao, L. Lin, Q. Zhou, Y. Li, S. Yuan, Q. Chen, S. Dong and J. Wang, *Nano letters*, 2018, **18**, 2943-2949.
3. C. Gong, L. Li, Z. Li, H. Ji, A. Stern, Y. Xia, T. Cao, W. Bao, C. Wang and Y. Wang, *Nature*, 2017, **546**, 265.
4. H. H. Downs, R. M. Buchanan and C. G. Pierpont, *Inorganic Chemistry*, 1979, **18**, 1736-1740.
5. M. E. Ziebel, L. E. Darago and J. R. Long, *Journal of the American Chemical Society*, 2018, **140**, 3040-3051.
6. L. Zhang, Z. Wang, B. Huang, B. Cui, Z. Wang, S. Du, H.-J. Gao and F. Liu, *Nano letters*, 2016, **16**, 2072-2075.